

Topological properties of tetratomic Su-Schrieffer-Heeger chains with hierarchical long-range hopping

Guan-Qiang Li(李冠强), Bo-Han Wang(王博涵), Jing-Yu Tang(唐劲羽), Ping Peng(彭娉), and Liang-Wei Dong(董亮伟)

Citation: Chin. Phys. B, 2023, 32 (**7**): 077102. DOI: 10.1088/1674-1056/aca7ef
Journal homepage: http://cpb.iphy.ac.cn; http://iopscience.iop.org/cpb

What follows is a list of articles you may be interested in

Coexistence of giant Rashba spin splitting and quantum spin Hall effect in H-Pb-F

Wenming Xue(薛文明), Jin Li(李金), Chaoyu He(何朝宇), Tao Ouyang(欧阳滔), Xiongying Dai(戴雄英), and Jianxin Zhong(钟建新)

Chin. Phys. B, 2023, 32 (**3**): 037101. DOI: 10.1088/1674-1056/aca7eb

First-principles prediction of quantum anomalous Hall effect in two-dimensional Co_2Te lattice

Yuan-Shuo Liu(刘元硕), Hao Sun(孙浩), Chun-Sheng Hu(胡春生), Yun-Jing Wu(仵允京), and Chang-Wen Zhang(张昌文)

Chin. Phys. B, 2023, 32 (**2**): 027101. DOI: 10.1088/1674-1056/aca082

SU(3) spin-orbit coupled fermions in an optical lattice

Xiaofan Zhou(周晓凡), Gang Chen(陈刚), and Suo-Tang Jia(贾锁堂)

Chin. Phys. B, 2022, 31 (**1**): 017102. DOI: 10.1088/1674-1056/ac11dc

Quantum anomalous Hall effect in twisted bilayer graphene quasicrystal

Zedong Li(李泽东) and Z F Wang(王征飞)†

Chin. Phys. B, 2020, 29 (**10**): 107101. DOI: 10.1088/1674-1056/abab77

Control of topological phase transitions in Dirac semimetal films by exchange fields

Fei Yang(杨菲), Hai-Long Wang(王海龙), Hui Pan(潘晖)

Chin. Phys. B, 2017, 26 (**1**): 017102. DOI: 10.1088/1674-1056/26/1/017102

Topological properties of tetratomic Su–Schrieffer–Heeger chains with hierarchical long-range hopping

Guan-Qiang Li(李冠强)†, Bo-Han Wang(王博涵), Jing-Yu Tang(唐劲羽), Ping Peng(彭娉), and Liang-Wei Dong(董亮伟)

Department of Physics and Institute of Theoretical Physics, Shaanxi University of Science and Technology, Xi'an 710021, *China*

(Received 24 October 2022; revised manuscript received 20 November 2022; accepted manuscript online 2 December 2022)

We propose a new generalized Su–Schrieffer–Heeger model with hierarchical long-range hopping based on a one-dimensional tetratomic chain. The properties of the topological states and phase transition, which depend on the cointeraction of the intracell and intercell hoppings, are investigated using the phase diagram of the winding number. It is shown that topological states with large positive/negative winding numbers can readily be generated in this system. The properties of the topological states can be verified by the ring-type structures in the trajectory diagram of the complex plane. The topological phase transition is strongly related to the opening (closure) of an energy bandgap at the center (boundaries) of the Brillouin zone. Finally, the non-zero-energy edge states at the ends of the finite system are revealed and matched with the bulk–boundary correspondence.

Keywords: generalized Su–Schrieffer–Heeger model, tight-binding approximation, topological phase transition, long-range hopping, winding number, edge state

PACS: 71.20.–b, 71.23.An, 68.65.–k, 73.43.Nq **DOI:** 10.1088/1674-1056/aca7ef

1. Introduction

The topological properties of matter have become a hot topics in the frontier of physics in recent years.[1,2] Several theoretical tools for characterizing the topological states under different situations have been established. For example, the Berry phase has been widely used in the study of the topological aspects of quantum states since it was first proposed.[3,4] Further development of this concept has produced the Berry curvature and the Berry connection,[5] which can be used to calculate the topological invariants of the topologically nontrivial states, such as the Chern number. In physics, the quantized transverse conductivity of the quantum Hall effect has a close relationship with the Chern number.[6] Using an effective numerical method, the Chern number in the discrete Brillouin zone can easily be calculated.[7] The Chern number can describe the topological properties of two-dimensional or higher-dimensional systems. One of the simplest nontrivial topological models is the Su–Schrieffer–Heeger (SSH) model proposed by Su, Schrieffer, and Heeger,[8] which was originally used to describe electron transport in one-dimensional (1D) polyacetylene. The so-called winding number is usually used to describe the topological properties of the 1D system, and the Zak phase plays an important role in calculating the winding number of the SSH model.[9] The SSH model, which is not as simple as it looks, has unusual physical connotations. In the past few decades, extensive studies have investigated the SSH model and its variants, such as an SSH model with next-nearest-neighbor hopping,[10–12] the SSH3 and SSH4 models with short- and long-range hopping,[13–21] an SSH model with spin–orbit coupling,[22,23] and two coupled SSH chains.[24–26]

The basic SSH model has two alternating hopping amplitudes that do not include the potential energy at the atomic sites.[27,28] Under periodic boundary conditions, the bulk–boundary correspondence indicates that there are two different regimes determined by the ratio of the two hopping amplitudes. Under open boundary conditions, the edge states are found at the boundaries of the system. Furthermore, the number of edge states at the boundaries has a one-to-one correspondence with the 1D winding number of the system. The SSH model has been experimentally implemented in a variety of physical platforms, such as 1D phononic crystals,[29,30] resonant coupled optical waveguides,[31] topolectrical circuits,[32,33] and even ultracold atomic gases interacting via optical lattices.[34,35] Following closely behind the Su–Schrieffer–Heeger (SSH) model, the topological properties of the generalized SSH models have been studied in recent years, such as the SSH4 model with four inequivalent atoms/sites per unit cell. The SSH4 model can introduce additional physics, since it offers additional internal degrees of freedom and a much wider parameter space.[36,37] The SSH model is hidden in the SSH4 chain if the latter's hopping amplitudes are suitably chosen. Due to the chiral symmetry of the Hamiltonian, the SSH4 model has the same classification of topological quantum states as the SSH model.[38] Recently, the SSH4 model was experimentally realized using ultracold atoms in a momentum lattice, and the topological phase transition was mapped by measuring the mean chiral displacement of the system.[39] The study of the topological

†Corresponding author. E-mail: liguanqiang@sust.edu.cn

© 2023 Chinese Physical Society and IOP Publishing Ltd

properties related to the SSH4 model has been given increasing attention. For example, some new theoretical progress has been made using the SSH4 model by considering the non-Hermiticity[40] or nonlinearity[41] of the system. However, many open problems still need to be investigated, such as the generalization of the SSH4 model by the addition of long-range hopping.

In this paper, we propose a new and realizable SSH4 model with hierarchical long-range hopping based on a 1D tetratomic chain. Our main results are as follows. (i) Topological states with large positive/negative winding numbers can readily be generated in the model by choosing suitable long-range hopping. The attainable magnitude of the winding number is determined by the highest order of the long-range hopping. A positive or negative winding number can be obtained by setting the hierarchical direction of the hopping. (ii) The boundaries of the quantum phase transition between topological states with different winding numbers are identified and can be controlled by both intracell and intercell hoppings. (iii) In addition to the near-zero-energy edge states, there are topologically protected edge states with energies greater than zero localized near the two ends of the system. The number of the edge states is the same as the winding number of the infinite system and completely matched with the bulk–boundary correspondence.[28]

The rest of the paper is organized as follows. In Section 2, the tight-binding model is presented and the corresponding real-space Hamiltonians for the infinite and finite systems are given. In Section 3, the Hamiltonian is transferred into the momentum space and the eigenvalues of the Hamiltonian are obtained for the infinite system. The method used to calculate the winding number using the eigenstates of the system is demonstrated. Section 4 gives the main results, including the winding number, the energy bands, the trajectory diagram for the infinite system, and the edge states for the finite system affected by the interactions between the intracell and intercell hopping. Finally, the conclusions are given in Section 5.

2. Model

The SSH4 model is a direct extension of the basic SSH model obtained by increasing the atom/site number per unit cell from two to four. Unlike the SSH3 model, the SSH4 model may have more exotic nontrivial topological properties due to its chiral symmetry.[18,19] Here, we provide a tetratomic SSH model with short- and long-range hopping based on a 1D atomic chain periodically formed from four inequivalent atoms per unit cell. The atoms are represented by A, B, C and D. The Hamiltonian of the tetratomic SSH model in the tight-binding approximation can be written as

$$H = \sum_{n\in Z}(t_{AB}a_n^\dagger b_n + t_{BC}b_n^\dagger c_n + t_{CD}c_n^\dagger d_n + \sum_{m\in Z} t_m d_n^\dagger a_{n+m}) + \text{h.c.}, \quad (1)$$

where $a_n^\dagger$, $b_n^\dagger$, $c_n^\dagger$ and $d_n^\dagger$ (a_n, b_n, c_n and d_n) are the atom's creation (annihilation) operators corresponding to A, B, C and D in the nth unit cell. In addition to the short-range interaction between adjacent atoms, only the long-range interaction between atoms D and A is considered in the model. In Eq. (1), t_{AB}, t_{BC}, t_{CD} and t_0 represent the intracell hopping amplitudes, t_1 denotes the amplitude of the intercell short-range hopping, and t_m $(m \in Z, m \neq 0, 1)$ represents the intercell long-range hopping. All the hopping amplitudes are assumed to be real. When several such long-range hopping events appear in the Hamiltonian at the same time, a system with staggered and hierarchical long-range hopping is obtained. In principle, our model can be used to analyze the physics of the SSH4 model with any order long-range hopping.

When a finite system with N unit cells is considered, the open boundary condition must be imposed. We define the integer $M \equiv \text{Max}(m)$ to represent the highest-order number of the long-range hopping. For a system with N unit cells and M-order hopping, $M < N$ must be satisfied. Taking $M = 3$ as an example, a model of the hierarchical long-range hopping can be obtained as follows:

$$\begin{aligned} H = & \sum_{n=1}^{N}(t_{AB}a_n^\dagger b_n + t_{BC}b_n^\dagger c_n + t_{CD}c_n^\dagger d_n + t_0 d_n^\dagger a_n) \\ & + \sum_{n=2}^{N} t_{-1}d_n^\dagger a_{n-1} + \sum_{n=3}^{N} t_{-2}d_n^\dagger a_{n-2} + \sum_{n=4}^{N} t_{-3}d_n^\dagger a_{n-3} \\ & + \sum_{n=1}^{N-1} t_1 d_n^\dagger a_{n+1} + \sum_{n=1}^{N-2} t_2 d_n^\dagger a_{n+2} + \sum_{n=1}^{N-3} t_3 d_n^\dagger a_{n+3} + \text{h.c.} \quad (2) \end{aligned}$$

A schematic diagram of a model that only considers $|m| \leq 3$ is given in Fig. 1. The hierarchical direction of the intercell long-range hopping related to t_m is rightward for $m > 1$, as shown in Fig. 1(a), while it is leftward for $m \leq -1$, as shown in Fig. 1(b). The rightward (leftward) hierarchical direction also corresponds to the positive (negative) phase of the hopping terms.

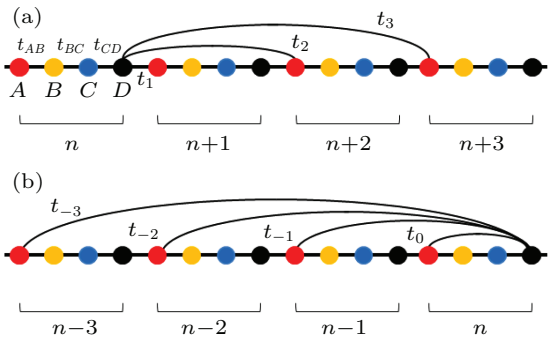


Fig. 1. Schematic diagram of the tetratomic SSH model with short- and long-range hopping for $M = 3$. Four atoms per unit cell in a 1D chain are represented by A (red), B (orange), C (blue) and D (black). t_{AB}, t_{BC}, t_{CD} and t_0 represent the intracell hopping amplitudes, while $t_{\pm1,\pm2,\pm3}$ denote the intercell hopping ones.

Assuming that $t_m = 0$ for $m \neq 1$, the model can be reduced to the SSH4 model.[36,40] When the infinite chain is considered, the system is topologically nontrivial for $t_1 t_{BC}/(t_{AB} t_{CD}) > 1$ and trivial for $t_1 t_{BC}/(t_{AB} t_{CD}) < 1$. When the finite chain is considered, edge states appear at the boundaries of the system. The properties of the edge states not only depend on the hopping amplitudes but also on the number of sites, which makes an analysis of the bulk–boundary correspondence complex.[42] Further, assuming that $t_{AB} = t_{CD}$ and $t_{BC} = t_1$, the model can be reduced to the basic SSH model.[8] The infinite system is topologically nontrivial for $t_{BC}/t_{AB} > 1$ and trivial for $t_{BC}/t_{AB} < 1$. The edge states of the finite system are mixing states and can be obtained from a superposition of the left- and right-handed states in which the zero energies are localized at the right and left boundaries of the semi-infinite system.[43] Our model is a generalization of the standard SSH4 model used to describe staggered and hierarchical long-range hopping. The exotic topological properties of the model can be numerically investigated using the energy band diagram, the winding number, and the edge states of the system once some analytical formulas have been obtained.

3. Methods

Taking the discrete Fourier transformation

$$(a_n, b_n, c_n, d_n) = \frac{1}{\sqrt{N}} \sum_{k \in Z} (a_k, b_k, c_k, d_k)\, \mathrm{e}^{-\mathrm{i}kn},$$

the Hamiltonian (2) can be transformed into

$$H(k) = \begin{pmatrix} 0 & t_{AB} & 0 & \sum_{m=-3}^{3} t_m \mathrm{e}^{-\mathrm{i}mk} \\ t_{AB} & 0 & t_{BC} & 0 \\ 0 & t_{BC} & 0 & t_{CD} \\ \sum_{m=-3}^{3} t_m \mathrm{e}^{\mathrm{i}mk} & 0 & t_{CD} & 0 \end{pmatrix} \tag{3}$$

in the momentum space for $N \to \infty$.[38] This Hamiltonian can also be considered to be a finite system with a periodic boundary condition. In addition to the term $t_1 \mathrm{e}^{-\mathrm{i}k}$ that appears in the SSH4 model, five intercell long-range hopping terms $t_{-1}\mathrm{e}^{\mathrm{i}k}$, $t_{\pm 2}\mathrm{e}^{\pm 2\mathrm{i}k}$ and $t_{\pm 3}\mathrm{e}^{\pm 3\mathrm{i}k}$ are presented in Eq. (3). The amplitudes and phases of the above hopping terms are chosen to reveal the exotic properties of the system, which are different from the physics discussed for the SSH4 model. The structure of the Hamiltonian can still be retained when M is increased. It can be seen that although our model looks very complicated for more hoppings, it does allow us to get some analytical results.

The tetratomic SSH model with hierarchical long-range hopping is protected by chiral symmetry, which is a combination of the time reversal and particle–hole symmetries and is defined in terms of an antiunitary operator Γ, which satisfies the equation $\Gamma^{\dagger} H(k) \Gamma = -H(k)$, with

$$\Gamma = \begin{pmatrix} -1 & 0 & 0 & 0 \\ 0 & 1 & 0 & 0 \\ 0 & 0 & -1 & 0 \\ 0 & 0 & 0 & 1 \end{pmatrix}. \tag{4}$$

Using a similarity transformation, Eq. (3) can be changed into an off-diagonal form, i.e.,

$$H(k) = \begin{pmatrix} 0 & g \\ g^{\dagger} & 0 \end{pmatrix}, \tag{5}$$

with

$$g(k) = \begin{pmatrix} t_{AB} & \sum_{m=-3}^{3} t_m \mathrm{e}^{-\mathrm{i}mk} \\ t_{BC} & t_{CD} \end{pmatrix}. \tag{6}$$

For the infinite system, the eigenvalues of the Hamiltonian (5) are calculated as follows:[18,36]

$$E(k) = \pm \sqrt{(T \pm \sqrt{T^2 - 4D})/2}, \tag{7}$$

where $T = t_{AB}^2 + t_{BC}^2 + t_{CD}^2 + M_1 M_2$ and $D = t_{AB}^2 t_{CD}^2 + M_1 M_2 t_{BC}^2 - (M_1 + M_2) t_{AB} t_{BC} t_{CD}$ with $M_1 = \sum_{m=-3}^{3} t_m \mathrm{e}^{-\mathrm{i}mk}$ and $M_2 = M_1^*$. The eigenstates with non-zero energy always appear in pairs with the eigenvalues $(E, -E)$, and the corresponding eigenstates are related by $|\Psi\rangle_- = \Gamma |\Psi\rangle_+$. The energy bandgaps based on the above eigenvalues at the center and boundaries of the Brillouin zone can be opened up or closed, depending on the hopping amplitudes chosen.

To simplify the analysis without losing the physics of the model, intracell hopping events with equal amplitudes, i.e., $t_{AB} = t_{BC} = t_{CD} \equiv t$, are considered hereinafter. The eigenvalues of the Hamiltonian are reduced to $E(k) = \pm[(M_0 + t) \pm \sqrt{M_0^2 - 2M_0 t + 5t^2}]$ with $M_0 = \sum_{m=-3}^{3} t_m$ at $k = 0$. Since the hopping amplitudes t and t_m can be adjusted, the bandgap at $k = 0$ can be closed if $M_0^2 - 2M_0 t + 5t^2 = 0$ or $M_0 = \pm t$ is satisfied. The bandgap can be similarly changed at the boundaries of the Brillouin zone, which depend on the lowest order of the intercell hopping. When the lowest-order intercell hopping $t_{\pm 1} \neq 0$, the boundaries of the Brillouin zone are at $k = \pm\pi$. The degeneracy of the eigenvalues of the Hamiltonian (gap closing) can be realized at the center or the boundaries of the Brillouin zone.

The winding number can be calculated to characterize the topological properties of the 1D system. The traditional method used for this calculation is to first calculate the Zak phase, since it is a gauge invariant quantity revised by the Wilson loop approach.[44,45] The winding number is related to the Zak phase by $W = \mathcal{Z}/2\pi$ for the SSH4 model. That is to say, the Zak phase can be guaranteed to be an accurate value under any phase change of the eigenstates: $\mathcal{Z} = \oint_{\mathrm{BZ}} \mathrm{i} \langle \psi_{n,k} | \partial_k \psi_{n,k} \rangle \mathrm{d}k$, where ψ_{nk} is the nth Bloch wavefunction. This definition can be converted into the following form: $\mathcal{Z} = -\mathrm{Im}\left[\log \prod_{k \in \mathrm{BZ}} \langle \psi_{n,k} | \psi_{n,k+\Delta k} \rangle\right]$, which is mainly

the value of the logarithm.[9,34] The result of this formula is no longer an integer multiple of 2π in the Brillouin zone because of the breaking of the inversion symmetry for the centered inversion axis of the system due to the the long-range hopping. A corrected quantized form of the Zak phase must be used by relating the Zak phase to the eigenvalues of the modified parity operators at the inversion invariant momenta.[20]

We use another effective method to obtain the winding number, which is expressed by the following formula:[36]

$$W = \frac{1}{2\pi \mathrm{i}} \int_{-\pi}^{\pi} \frac{\mathrm{d}\log[\mathrm{Det}(g)]}{\mathrm{d}k} \mathrm{d}k. \tag{8}$$

The calculation of the winding number performed using this formula does not need information about the eigenstates, but is directly determined by the structure of the Hamiltonian. A 1D model is topologically trivial or topologically nontrivial, depending on whether the winding number is zero or not. Physically, the formula can be understood by examining the ring-type structure of the trajectory diagram in the complex plane, which is constructed by plotting the real part of the determinant $G \equiv \mathrm{Det}(g)$ against its imaginary part. The number of times that the trajectory in the complex plane winds around the origin as k goes from $-\pi$ to π in the Brillouin zone corresponds to the winding number. The winding number is taken to be positive (negative) when the trajectory winds around the origin counterclockwise (clockwise). The topological properties of the system can be described effectively by the formula due to the symmetry of the Hamiltonian.

4. Main results

The topological properties and phase transitions are investigated using the phase diagrams of the winding number for the two selected intercell hoppings. In Fig. 2(a), the change of the winding number with the hopping amplitudes t_1 and t_2 is given for the intracell hopping amplitude $t = 1.0$ and the other amplitudes $t_m = 0$ with $m \neq 1, 2$. The phase plane is divided into five regions, in which two regions represent $W = 2$, two regions represent $W = 1$ and one region represents $W = 0$. The region that represents $W = 0$, which corresponds to the topologically trivial phase, is a triangle and is located in the central region of the plane. The regions that represent $W \neq 0$ correspond to the topologically nontrivial phases and occupy most of the plane. The two regions that represent $W = 1$ are distributed symmetrically about the axis given by $t_1 = 0$. The two regions that represent $W = 2$ are distributed on the upper and lower sides of the plane related to $t_2 > 0$ and $t_2 < 0$. The area of the region corresponding to $t_2 > 0$ is smaller than that of the region corresponding to $t_2 < 0$. This asymmetry is caused by the existence of $t = 1.0$ when t_1 and t_2 are competing. If the amplitudes are tuned from one region to the another with a different winding number, a topological phase transition occurs. In Fig. 2(b), a change of the winding number with t_1 and t_3 is shown for $t = 1.0$ and the other amplitudes $t_m = 0$ with $m \neq 1, 3$. The plane is divided into seven regions, including two regions for $W = 3$, two regions for $W = 2$, two regions for $W = 1$, and one region for $W = 0$. The central region for $W = 0$ is a quadrangle with two straight sides and two curved ones. The plane is no longer distributed symmetrically against the axis $t_1 = 0$, but has a symmetry determined by the chiral symmetry of the Hamiltonian. More importantly, it is found that the topological states with high winding numbers can be produced by suitably choosing the hopping terms.

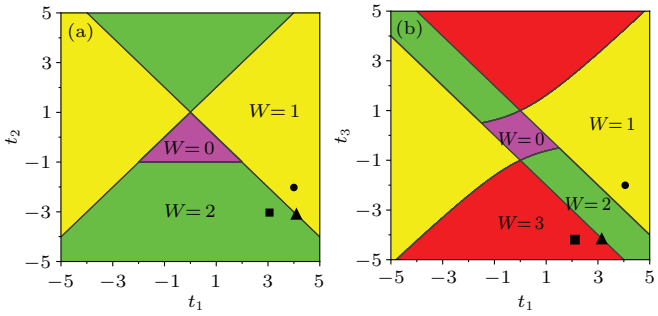


Fig. 2. The change of the winding number with the intercell hopping amplitudes t_1 and t_2 in (a) and t_1 and t_3 in (b) for the given intracell hopping amplitudes $t = 1.0$ and the other amplitudes $t_m = 0$. The regions corresponding to the topological states with the winding numbers $W = 0$, $W = 1$, and $W = 2$ are represented by magenta, yellow, and green in (a) and (b). The region corresponding to $W = 3$ is represented by red in (b). Three markers in (a) and (b) are selected to demonstrate the energy bands and the trajectory diagrams of the complex planes in Figs. 3 and 4. The circular and square markers are placed in the regions with $W = 1$ and $W = 2$, respectively. The triangular marker is placed at the boundary between the $W = 1$ and $W = 2$ regions.

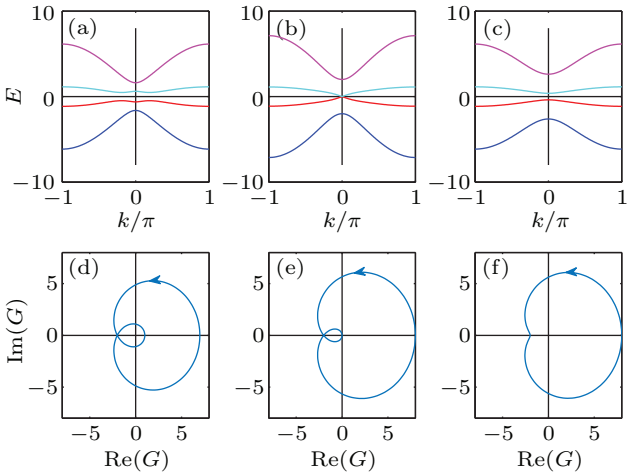


Fig. 3. (a)–(c) Energy bands and (d)–(f) trajectory diagrams of the complex plane (Re(G), Im(G)) are used to verify the topological properties shown in Fig. 2(a). In (a) and (d), the amplitudes of the hopping events are $t_1 = 3.0$ and $t_2 = -3.0$, which correspond to the square marker in Fig. 2(a). In (b) and (e), the amplitudes of the hopping events are $t_1 = 4.0$ and $t_2 = -3.0$, which correspond to the triangle marker in Fig. 2(a). In (c) and (f), the amplitudes of the hopping events are $t_1 = 4.0$ and $t_2 = -2.0$, which correspond to the circular marker in Fig. 2(a).

The topological phase transition is strongly related to the opening or closure of the energy bandgap at the center/boundaries of the Brillouin zone. Figures 3(a)–3(c) give

the energy bands of the system for three different sets of hopping amplitudes, which are represented by three different markers in Fig. 2(a). The square, triangular, and circular makers correspond to the sets of amplitudes ($t_1 = 3.0$, $t_2 = -3.0$), ($t_1 = 4.0$, $t_2 = -3.0$), and ($t_1 = 4.0$, $t_2 = -2.0$), respectively. There are four energy bands $E_{1,2,3,4}(k)$ in all cases due to the number of sites per unit cell. The bandgap is opened up both at the center and the boundaries of the Brillouin zone in Figs. 3(a) and 3(c), but closed at the center of the Brillouin zone in Fig. 3(b) due to $E_2(k=0) = E_3(k=0)$. A topological phase transition occurs when the bandgap of the Hamiltonian changes from open to closed or vice versa. The topological properties can also be verified by the ring-type structures in the trajectory diagram of the complex plane corresponding to (Re(G), Im(G)). Figures 3(d)–3(f) shows trajectory diagrams of the complex plane corresponding to the energy bands shown in Figs. 3(a)–3(c). The trajectory diagram in the complex plane winds anticlockwise around the origin two, one, and one times in Figs. 3(d)–3(e) and the relevant winding numbers are 2, 1, and 1, respectively. Figures 3(b) and 3(e) show the critical situation for the phase transition between $W = 1$ and $W = 2$.

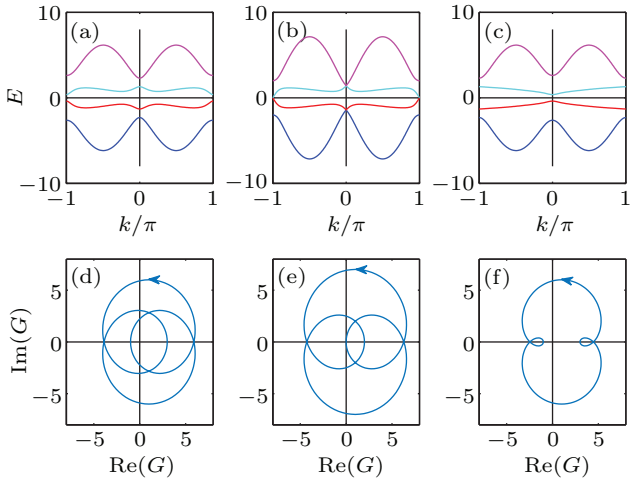


Fig. 4. (a)–(c) Energy bands and (d)–(f) trajectory diagrams of the complex plane (Re(G), Im(G)) about G are used to verify the topological properties shown in Fig. 2(b). In (a) and (d), the amplitudes of the hopping events are $t_1 = 2.0$ and $t_3 = -4.0$, which correspond to the square marker in Fig. 2(b). In (b) and (e), the amplitudes of the hopping events are $t_1 = 3.0$ and $t_3 = -4.0$, which correspond to the triangle marker in Fig. 2(b). In (c) and (f), the amplitudes of the hopping events are $t_1 = 4.0$ and $t_3 = -2.0$, which correspond to the circular marker in Fig. 2(b).

Similar results can be obtained for the case of $t_1 \neq 0$ and $t_3 \neq 0$ shown in Fig. 2(b). Figures 4(a)–4(c) gives the energy bands of the system for the three different sets of hopping amplitudes marked in Fig. 2(b). The square, triangular, and circular makers correspond to the sets of amplitudes ($t_1 = 2.0$, $t_3 = -4.0$), ($t_1 = 3.0$, $t_3 = -4.0$), and ($t_1 = 4.0$, $t_3 = 2.0$), respectively. The bandgap is opened up both at the center and the boundaries of the Brillouin zone in Figs. 4(a) and 4(c), but is closed at the center and the boundaries of the Brillouin zone in Fig. 4(b) due to $E_1(k=0) = E_2(k=0)$, $E_3(k=0) = E_4(k=0)$, and $E_2(k=\pm\pi) = E_3(k=\pm\pi)$. Figures 4(d)–4(f) give the corresponding results for the trajectory diagrams. The diagrams in the complex plane wind anticlockwise around the origin three, two, and two times in Figs. 4(d)–4(f) and the relevant winding numbers are 3, 2, and 2, respectively. Figures 4(b) and 4(e) show the critical situation for the phase transition between $W = 2$ and $W = 3$. The above results show that the energy bands and the trajectory diagram play very important roles in the identification of the topological properties of the system.

If a system with hierarchical long-range hopping is considered bidirectionally, topological states with positive and negative winding numbers can be generated, as demonstrated in Fig. 5. In Fig. 5(a), the change of the winding number with t_1 and t_2 is given for $t_m = 0$ with $m \neq 1, 2$. The region representing $W = 0$ is split into three parts. The regions with positive and negative winding numbers are generated in the same system by the different hopping amplitudes. The trajectory diagram winds clockwise around the origin for states with a negative winding number and counterclockwise around the origin for those with a positive winding number. Two regions with $W = -1$ and one region with $W = -2$ appear in the phase diagram. The regions with different winding numbers are distributed symmetrically about the axis $t_1 = 0$ due to $t_2 = t_{-2}$. In Fig. 5(b), the change of the winding number with t_1 and t_3 is demonstrated for $t_m = 0$ with $m \neq 1, 3$. Three regions with $W = \pm 1$, one region with $W = -2$, and one region with $W = -3$ appear in the phase diagram. There are also two regions for $W = 0$, 2, and 3, respectively. This case does not have the same symmetry as that shown in Fig. 5(a) due to the selected hopping amplitudes. Topological states with positive and negative winding numbers are created in the system, although only the two hopping amplitudes t_1 and t_3 are considered. The highest order of the long-rang hopping determines the complexity of the phase space for the winding number in the parameter space.

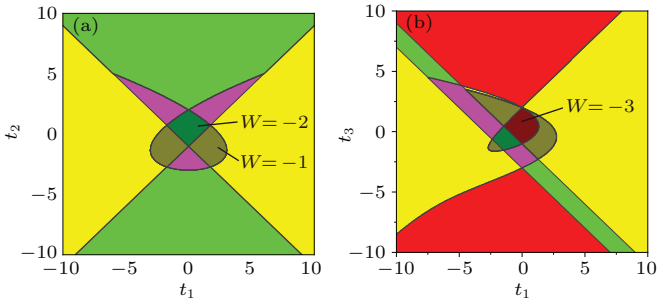


Fig. 5. The change of the winding number with t_1 and t_2 in (a) for the long-range hopping amplitudes $t_2 = t_{-2}$ and the other amplitudes $t_m = 0$ ($m \neq 1, \pm 2$) and with t_1 and t_3 in (b) for the long-range hopping amplitudes $t_3 = t_{-3}$ and the other amplitudes $t_m = 0$ ($m \neq 1, \pm 3$). The dark yellow and olive green regions represent topological states corresponding to $W = -1$ and $W = -2$ in (a). The claret-red region represents the topological states with $W = -3$ in (b). The other color settings are the same as those shown in Fig. 2.

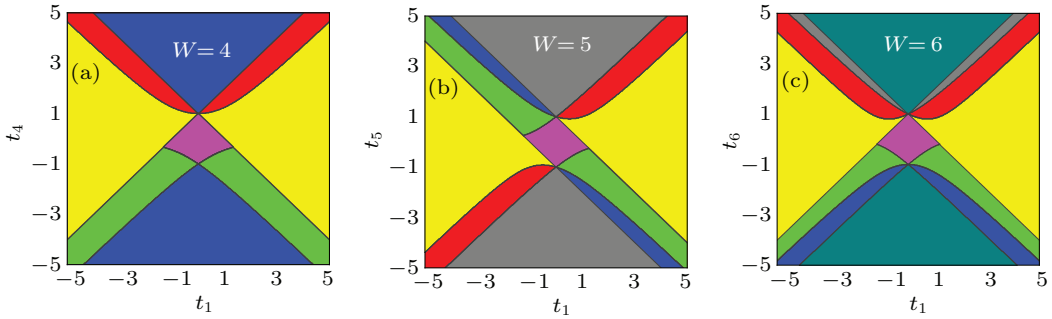


Fig. 6. The change of the winding number with t_1 and t_4 in (a), t_1 and t_5 in (b), and t_1 and t_6 in (c) for $t = 1.0$ and the other amplitudes $t_m = 0$.

To investigate the topological properties of systems with large winding numbers, higher-order intercell long-range hoppings are introduced. Figure 6 gives the phase diagrams for the winding number in the phase planes of (t_1, t_4) in (a), (t_1, t_5) in (b), and (t_1, t_6) in (c), keeping the other amplitudes $t_m = 0$. The largest winding numbers for the topological states are $W = 4$ in Fig. 6(a), $W = 5$ in Fig. 6(b), and $W = 6$ in Fig. 6(c). Regions representing $W = 4$ (blue) in Fig. 6(a), $W = 5$ (gray) in Fig. 6(b), and $W = 6$ (dark cyan) in Fig. 6(c) appear and occupy large areas in the relevant parameter spaces. The winding numbers for all regions are no smaller than zero. If we use the amplitudes $(t_1, t_{-4,-5,-6})$ as the parameters with which to construct the phase plane, the topological states with the largest winding numbers, i.e., $W = -4, -5$, and -6, can be created. Correspondingly, the winding numbers for all regions are no larger than zero. Theoretically, a topological state with a large positive/negative winding number can be realized once a suitable hopping amplitude is chosen. The parity of the phase diagram around the axis $t_1 = 0$ depends on whether the highest order of the hopping is odd or even. The phase diagram is symmetric around the axis $t_1 = 0$ for the highest-order long-range hopping, but not for odd orders of hopping. This result also holds for the higher-order long-range interactions, due to the symmetry of the Hamiltonian.

Intracell hopping plays an important role in the generalization of the topological states. Figures 7(a) and 7(b) investigate the effects of intracell hopping t on the topological properties in the above model by choosing the hopping amplitudes $t = 3.0$ and 5.0. The results for the same parameters except $t = 1.0$ are shown in Fig. 2(a). This shows that the larger the intracell hopping amplitude t, the larger the central region with the winding number $W = 0$. The other regions also correspondingly expand with increasing t in the phase plane. The role of the intracell hopping is not helpful for the generation of nontrivial topological states. The effect of the intracell hopping t_0 on the winding number is similar to that of t, except for the existing singularity in the calculation of the winding number at $t = t_0$.

We now investigate the properties of the edge states for the finite system under open boundary conditions. The number of unit cells in the system is set to $N = 25$, and the number of the atoms/sites is 100. There are no zero-energy eigenstates strictly localized at the left (right) boundary of the system, which corresponds to the right-handed (left-handed) state for the semi-infinite system.[43,44] Here, all of the edge states are superpositions of the left- and right-handed eigenstates, since quantum tunneling must be considered for the finite system. Since they have the characteristics of exponential decay, the edge states are mainly distributed near the two ends of the finite system. Such topologically protected edge states related to different winding numbers can be obtained by adjusting the intercell hopping amplitudes.

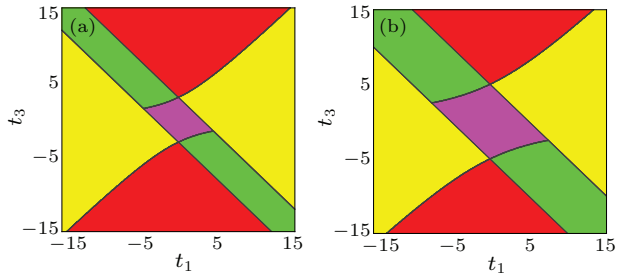


Fig. 7. The change of the winding number with t_1 and t_3 for $t = 3.0$ in (a) and $t = 5.0$ in (b), while for the other amplitudes, $t_m = 0$ and $m \neq 0, 1$.

Figure 8 shows the eigenvalues and the edge states of the finite system when the intercell hopping amplitudes chosen are $t_1 = 1.0$, $t_3 = -4.0$ and the other amplitudes $t_m = 0$ for $m \neq 0, 1$. Under these parameter conditions, the winding number of the topological states for the infinite system is $W = 3$. The changes of the eigenvalues with the state indexes are shown in Fig. 8(a). This figure shows that eigenstates with nonzero energy appear in pairs in which the two eigenvalues are opposite in sign. Six states Ψ_i $(i = 48, 49, 50, 51, 52, 53)$ have near-zero energy eigenvalues $E_v \simeq -0.0448$, -6.33×10^{-7}, -9.86×10^{-8}, 9.86×10^{-8}, 6.33×10^{-7}, 0.0448, among which three $(\Psi_i\ (i = 48,\ 49,\ 50))$ or $(\Psi_i\ (i = 51,\ 52,\ 53))$ are inequivalent, since the corresponding wave functions have different distributions along the sites. The distributions of the three near-degenerate and inequivalent edge states with the sites are shown in Figs. 8(b)–8(d), respectively. The distributions of the edge state have even/odd parity along the

sites for the even/odd state index, which is caused by the symmetric/asymmetric superposition of the left- and right-handed states with zero-energy eigenvalues. More importantly, there are twelve non-zero-energy edge states in the system, which are represented by Ψ_i $(i = 23,24,25,26,27,28)$ and Ψ_i $(i = 73,74,75,76,77,78)$ and have the energies $E_v \simeq -1.43,-1.41,-1.41,-1.41,-1.41,-1.39$ and $E_v \simeq 1.39,1.41,1.41,1.41,1.41,1.43$, respectively. The six inequivalent non-zero-energy edge states have similar distributions along the sites to those of the near-zero-energy edge states, but their energies are greater than zero. The wave function of each edge state is localized near the two ends of the system. Unlike the near-zero-energy edge states, the non-zero-energy edge states are not topologically protected by the chiral symmetry of the system but by the specific symmetry that folds the spectrum around these finite energies.[20]

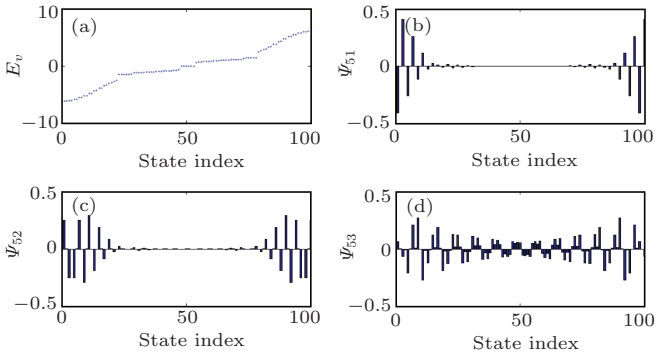


Fig. 8. Eigenvalues E_v and the edge states Ψ_i $(i = 51, 52, 53)$ for the finite system corresponding to $W = 3$ are shown. The hopping amplitudes $t_1 = 1.0$ and $t_3 = -4.0$ are selected.

Figure 9 shows the eigenvalues and the edge states of the finite system when the intercell hopping amplitudes chosen are $t_1 = 1.0$ and $t_5 = 4.0$ and the other amplitudes $t_m = 0$ for $m \neq 0,1$. The winding number of the topological states for the infinite system is $W = 5$. The changes of the eigenvalues with the state indexes are shown in Fig. 9(a). There are ten states, Ψ_i $(i = 46, 47, 48, 49, 50, 51, 52, 53, 54, 55)$, which have near-zero-energy eigenvalues $E_v \simeq -0.0220$, -0.0015, -0.0014, -9.04×10^{-6}, 9.04×10^{-6}, 0.0014, 0.0015, 0.0220, 0.0346, among which, five Ψ_i $(i = 46, 47, 48, 49, 50)$ or Ψ_i $(i = 51, 52, 53, 54, 55)$ are inequivalent to each other, since the corresponding wave functions have different distributions along the sites. The five near-degenerate edge states with the site indexes are shown in Figs. 9(b)–9(f), respectively. There are twenty non-zero-energy edge states, which are represented by Ψ_i $(i = 21,22,23,24,25,26,27,28,29,30)$ and Ψ_i $(i = 71,72,73,74,75,76,77,78,79,80)$ which have energies of $E_v \simeq -1.4302$, -1.4245, -1.4150, -1.4149, -1.4142, -1.4142, -1.4135, -1.4134, -1.4024, -1.3952 and $E_v \simeq 1.3952$, 1.4024, 1.4134, 1.4135, 1.4142, 1.4142, 1.4149, 1.4150, 1.4245, 1.4302, respectively. The wave functions of each edge state are also localized near the two ends of the system. The features of the states follow the bulk–boundary correspondence. Compared to Fig. 8, it can be seen that when the winding number is five, the number of inequivalent edge states is five. In contrast to the edge states, the wave function of the extended states is distributed at all sites.

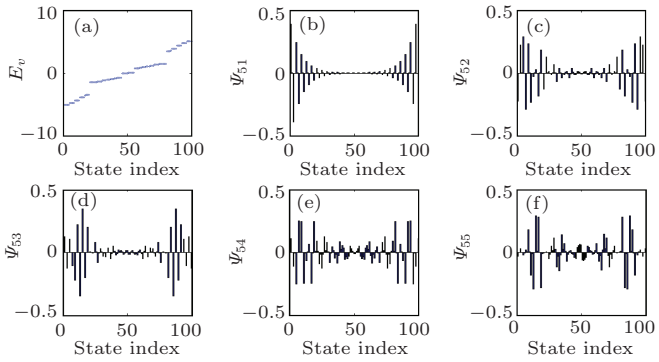


Fig. 9. Eigenvalues E_v and the edge states Ψ_i $(i = 51, 52, 53, 54, 55)$ for the finite system corresponding to $W = 5$ are shown. The hopping amplitudes $t_1 = 1.0$ and $t_5 = 4.0$ are selected.

5. Conclusions

In summary, we have investigated the topological properties of a tetratomic SSH model that introduces four inequivalent atoms per unit cell by adding long-range hopping. The topological properties and phase transition were investigated by examining phase diagrams of the winding numbers, the energy bands, and trajectory diagrams in the complex plane. The system has very rich phase diagrams, depending on the hopping choices. The effects of the short- and long-range hopping on the topological phase transition were investigated in detail. Under open boundary conditions, we confirmed that the number of edge states corresponding to the different winding numbers follows the bulk–boundary correspondence. Although the model with more hopping terms looks very complicated, most of the topological properties of the system were analyzed using conventional methods for the topological states. The model discussed here is universal and can be generalized to any order of the long-range hopping; it is applicable to a variety of physical platforms, such as electrical circuits and ultracold atoms trapped in optical lattices. Our work provides a new SSH-type model that enriches research into the topological properties of low-dimensional quantum systems and can be realized in forthcoming experiments.

Acknowledgements

Project supported by the National Natural Science Foundation of China (Grant No. 11405100), the Natural Science Basic Research Program in Shaanxi Province of China (Grant Nos. 2022JZ-02, 2020JM-507, and 2019JM-332), the Doctoral Research Fund of Shaanxi University of Science and Technology in China (Grant Nos. 2018BJ-02 and 2019BJ-58), and the Youth Innovation Team of Shaanxi Universities.

References

[1] Hasan M Z and Kane C L 2010 *Rev. Mod. Phys.* **82** 3045
[2] Qi X L and Zhang S C 2011 *Rev. Mod. Phys.* **83** 1057
[3] Berry M V 1984 *Proc. R. Soc. Lond A* **392** 45
[4] Xiao D, Chang M C and Niu Q 2010 *Rev. Mod. Phys.* **82** 1959
[5] Cooper N R, Dalibard J and Spielman I B 2019 *Rev. Mod. Phys.* **91** 015005
[6] Thouless D J, Kohmoto M, Nightingale M P and den Nijs M 1982 *Phys. Rev. Lett.* **49** 405
[7] Fukui T, Hatsugai Y and Suzuki H 2005 *J. Phys. Soc. Jpn.* **74** 1674
[8] Su W P, Schrieffer J R and Heeger A J 1979 *Phys. Rev. Lett.* **42** 1698
[9] Zak J 1989 *Phys. Rev. Lett.* **62** 2747
[10] Li L, Xu Z and Chen S 2014 *Phys. Rev. B* **89** 085111
[11] Rufo S, Lopes N, Continentino M A and Griffith M A R 2019 *Phys. Rev. B* **100** 195432
[12] Pérez-González B, Bello M, Gómez-Leṕn Á and Platero G 2019 *Phys. Rev. B* **99** 035146
[13] Martinez Alvarez V M and Coutinho-Filho M D 2019 *Phys. Rev. A* **99** 013833
[14] Anastasiadis A, Styliaris G, Chaunsali R, Theocharis G and Diakonos F K 2022 *Phys. Rev. B* **106** 085109
[15] Guo H M and Chen S 2015 *Phys. Rev. B* **91** 041402
[16] Eliashvili M, Kereselidze D, Tsitsishvili G and Tsitsishvili M 2017 *J. Phys. Soc. Jpn.* **86** 074712
[17] Marques A M and Dias R G 2020 *J. Phys. A: Math. Theor.* **53** 075303
[18] He Y and Chien C C 2021 *J. Phys.: Condens. Matter* **33** 085501
[19] Zhang Y, Ren B, Li Y and Ye F 2021 *Opt. Express* **29** 42827
[20] Marques A M and Dias R G 2019 *Phys. Rev. B* **100** 041104
[21] Nehra R and Roy D 2022 *Phys. Rev. B* **105** 195407
[22] Bahari M and Hosseini M V 2020 *Physica E* **119** 113973
[23] Ahmadi N, Abouie J and Baeriswyl D 2020 *Phys. Rev. B* **101** 195117
[24] Li C, Lin S, Zhang G and Song Z 2017 *Phys. Rev. B* **96** 125418
[25] Zhao X L, Chen L B, Fu L B and Yi X X 2020 *Ann. Phys. (Berlin)* **532** 1900402
[26] Borja C, Gutiérrez E and López A 2022 *J. Phys.: Condens. Matter* **34** 205701
[27] Shen S Q 2017 *Topological insulators: Dirac equation in condensed matters* (2nd edn.) (Singapore: Springer Nature) p. 81
[28] Asbóth J K, Oroszlany L and Pályi A 2016 *A short course on topological insulators: Band-structure topology and edge states in one and two dimensions* (Lecture Notes in Physics, Vol. 919) (Springer Cham)
[29] Xiao M, Ma G, Yang Z, Sheng P, Zhang Z Q and Chan C T 2015 *Nat. Phys.* **11** 240
[30] Li X, Meng Y, Wu X, Yan S, Huang Y, Wang S and Wen W 2018 *Appl. Phys. Lett.* **113** 203501
[31] Zhu X Y, Wang H Q, Gupta S K, Zhang H J, Xie B Y, Lu M H and Chen Y F 2020 *Phys. Rev. Research* **2** 013280
[32] Lee C H, Imhof S, Berger C, Bayer F, Brehm J, Molenkamp L W, Kiessling T and Thomale R 2018 *Commun. Phys.* **1** 39
[33] Liu S, GaoW, Zhang Q, Ma S, Zhang L, Liu C, Xiang Y J, Cui T J and Zhang S 2019 *Research* **2019** 8609875
[34] Atala M, Aidelsburger M, Barreiro J T, Abanin D, Kitagawa T, Demler E and Bloch I 2013 *Nat. Phys.* **9** 795
[35] Meier E J, An F A and Gadway B 2016 *Nat. Commun.* **7** 13986
[36] Maffei M, Dauphin A, Cardano F, Lewenstein M and Massignan P 2018 *New J. Phys.* **20** 013023
[37] Bid S and Chakrabarti A 2022 *Phys. Lett. A* **423** 127816
[38] Chiu C K, Teo J C Y, Schnyder A P and Ryu S 2016 *Rev. Mod. Phys.* **88** 035005
[39] Xie D, Gou W, Xiao T, Gadway B and Yan B 2019 *npj Quantum Inf.* **5** 55
[40] Li J R, Zhang L L, Cui W B and Gong W J 2022 *Phys. Rev. Research* **4** 023009
[41] Zhou X F, Pan J S and Jia S T 2023 *Phys. Rev. B* **107** 054105
[42] Lee C S, Io I F and Kao H C 2022 *Chin. J. Phys.* **78** 96
[43] Chen H T, Chang C H and Kao H C 2021 *Chin. J. Phys.* **72** 50
[44] Zurita J, Creffield C and Platero G 2019 *Adv. Quantum Technol.* **3** 1900105
[45] Wang H X, Guo G Y and Jiang J H 2019 *New J. Phys.* **21** 093029